CrossMark

ORIGINAL ARTICLE

Orbital dynamics and equilibrium points around an asteroid with gravitational orbit–attitude coupling perturbation

Yue Wang[1] · **Shijie Xu[2]**

Abstract The strongly perturbed dynamical environment near asteroids has been a great challenge for the mission design. Besides the non-spherical gravity, solar radiation pressure, and solar tide, the orbital motion actually suffers from another perturbation caused by the gravitational orbit–attitude coupling of the spacecraft. This gravitational orbit–attitude coupling perturbation (GOACP) has its origin in the fact that the gravity acting on a non-spherical extended body, the real case of the spacecraft, is actually different from that acting on a point mass, the approximation of the spacecraft in the orbital dynamics. We intend to take into account GOACP besides the non-spherical gravity to improve the previous close-proximity orbital dynamics. GOACP depends on the spacecraft attitude, which is assumed to be controlled ideally with respect to the asteroid in this study. Then, we focus on the orbital motion perturbed by the non-spherical gravity and GOACP with the given attitude. This new orbital model can be called *the attitude-restricted orbital dynamics*, where *restricted* means that the orbital motion is studied as a restricted problem at a given attitude. In the present paper, equilibrium points of the attitude-restricted orbital dynamics in the second degree and order gravity field of a uniformly rotating asteroid are investigated. Two kinds of equilibria are obtained: on and off the asteroid equatorial principal axis. These equilibria are different from and more diverse than those in the classical orbital dynamics without GOACP. In the case of a large spacecraft, the off-axis equilibrium points can exist at an arbitrary longitude in the equatorial plane. These results are useful for close-proximity operations, such as the asteroid body-fixed hovering.

✉ Yue Wang
ywang.buaa@gmail.com

Shijie Xu
starsjxu@163.com

[1] Distributed Space Systems Lab, Faculty of Aerospace Engineering, Technion – Israel Institute of Technology, 32000 Haifa, Israel

[2] School of Astronautics, Beihang University, Beijing 100191, China

 Springer

1 Introduction

The strongly perturbed dynamical environment in the proximity of small asteroids has been a great challenge for the mission design, navigation, and control. To have a thorough understanding of the dynamical behavior, the spacecraft dynamics about asteroids have been studied broadly, including the orbital dynamics, attitude dynamics, and the gravitationally coupled orbit–attitude dynamics (full dynamics).

Many works have focused on the orbital dynamics near asteroids, such as Scheeres (1994, 2012a, b, 2014), Hu (2002), Hu and Scheeres (2004), Liu et al. (2011a, b), Russell (2012), Yu and Baoyin (2012a, b, 2013), Li et al. (2013), Jiang et al. (2014), Llanos et al. (2014), and so on. It has been found that the orbital motion is strongly perturbed by the non-spherical gravity of the asteroid, solar radiation pressure (SRP) and solar tide. Stable orbits against these multiple perturbations should be constructed carefully with analytical approaches and numerical tests (Scheeres 2012a, b).

Several works have studied the attitude dynamics of spacecraft around asteroids, such as Riverin and Misra (2002), Misra and Panchenko (2006), Kumar (2008), Wang and Xu (2013a, b), and Zhang and Zhao (2014, 2015). These results have shown that the attitude motion is perturbed strongly by the non-spherical mass distribution and rotation of the asteroid, and the attitude stability domain is modified remarkably in comparison with, even totally different from, the classical stability domain in a central gravity field.

In the close proximity of a small asteroid, due to the large ratio of the spacecraft dimension to the orbit radius, there is a significant gravitational coupling between the orbit and attitude motions of a large spacecraft, as shown by Wang and Xu (2014a). The magnitude of gravitational orbit–attitude coupling can be estimated by $\varepsilon = \rho/r_0$, where ρ is the spacecraft characteristic dimension and r_0 is the orbital radius (Sincarsin and Hughes 1983). For a spacecraft ($\rho \sim 10\,\text{m}$) around Earth, ε is order of 10^{-6}. However, for a spacecraft around a small asteroid, ε can be several orders of magnitude larger due to the small size of the asteroid and the resulting small orbit radius. Therefore, the traditional spacecraft dynamics, in which the orbit and attitude motions are treated separately, will no longer maintain a high precision.

The gravitationally coupled orbit-attitude dynamics, which can be also called *the full dynamics*, has been proposed to take into account the gravitational orbit-attitude coupling with the spacecraft modeled as an extended rigid body. The gravitationally coupled orbit–attitude dynamics (full dynamics) of a rigid spacecraft has been studied qualitatively in a central gravity field (Wang et al. 1991, 1992; Sanyal 2004; Teixidó Román 2010), as well as in a J_2-truncated gravity field of a small spheroid asteroid (Wang and Xu 2013c, d; Wang et al. 2014a), and in the second degree and order gravity field of a uniformly rotating asteroid described with the harmonic coefficients C_{20} and C_{22} (Wang and Xu 2014b; Wang et al. 2014b). These studies have mainly focused on the general qualitative properties of the system, including the relative equilibria and their stability. The coupled orbit–attitude dynamics of a rigid spacecraft has been used in the control and navigation of the close-proximity operations near asteroids (Lee et al. 2014; Sanyal et al. 2014; Misra et al. 2015).

The gravitationally coupled orbit–attitude motions of small celestial bodies has been studied in the full two body problem (F2BP), i.e., two rigid bodies orbiting each other interacting through the mutual gravitational potential (Scheeres 2004, 2006, 2009; Fahnestock and

Scheeres 2008; McMahon and Scheeres 2013; Woo et al. 2013). Notice that although the orbit–attitude coupling has been adopted in the dynamics of high area-to-mass ratio space debris (Früh et al. 2013) and the relative dynamics of spacecraft (Segal and Gurfil 2009), these couplings have different physical origins, and should not be confused with the gravitational orbit–attitude coupling.

Although the gravitationally coupled orbit–attitude dynamics has been proposed and studied, if from the viewpoint of orbital dynamics, the gravitational orbit–attitude coupling of the spacecraft actually causes another orbital perturbation to the Kepler two-body problem besides the non-spherical gravity of the asteroid, SRP and solar tide. This gravitational orbit–attitude coupling perturbation (GOACP) depends on the spacecraft attitude and has its origin in the fact that the gravity acting on a non-spherical extended body, the real case of the spacecraft, is actually different from that acting on a point mass, the model of the spacecraft in the orbital dynamics. In this paper, we will show that GOACP and the non-spherical terms of the asteroid's gravity are both second-order terms of the gravitational force. Because of the dynamical sensitivity, GOACP needs to be considered for a large spacecraft.

Due to GOACP, the previous close-proximity orbital dynamics, in which only the non-spherical gravity is considered, will no longer have a high precision for a large spacecraft. If GOACP is neglected, as an unmodeled perturbation, it will degenerate the control accuracy, and fuel will be needed to null out its effect. If it is taken into account, the dynamics will be revealed better, and the fuel consumption will be more effective. That is, fuel can be saved by considering GOACP.

Therefore, we intend to take into account GOACP in the close-proximity orbital dynamics besides the non-spherical gravity. Since GOACP depends on the spacecraft attitude, we assume that the spacecraft is controlled ideally to a given attitude with respect to the asteroid, and then we focus on the orbital motion perturbed by the non-spherical gravity and GOACP with the given attitude. This new orbital model can be called *the attitude-restricted orbital dynamics*, where *restricted* means that the orbital motion is studied as a restricted problem at a given attitude.

The traditional spacecraft dynamics and the attitude-restricted orbital dynamics are two different approximations of the exact spacecraft motion. In the former, the spacecraft is first treated as a point mass in the orbital dynamics and the attitude motion is treated as a restricted problem on the predetermined orbit, whereas, in the latter, the spacecraft attitude is first given and the orbital motion is treated as a restricted problem at the predetermined attitude. The traditional dynamics is applicable when the spacecraft is small in comparison with the orbital radius and GOACP is negligible, such as around Earth, planets, and other large celestial bodies. The attitude-restricted orbital dynamics is applicable near a small asteroid or comet when GOACP is significant and the attitude can be controlled ideally.

Besides providing a more precise orbital model, the attitude-restricted orbital dynamics is also reasonable from the viewpoint of space engineering. Notice that the gravity gradient torque caused by the asteroid is small and can be well stabilized by using the attitude control system. In space engineering, a strong control of the spacecraft attitude against exterior perturbations can be achieved at the cost of electricity, which can be generated by solar panels, whereas the orbital control is much weaker, and the natural orbital dynamics need to be fully utilized for the purpose of saving fuel, since the fuel is more limited than the electricity.

Because of GOACP, the phase space of attitude-restricted orbital dynamics will be different from and more complicated than that of previous close-proximity orbital dynamics. In the present paper, we will give a qualitative study of attitude-restricted orbital dynamics. Equations of motion will be obtained and equilibrium points will be investigated as well. These equilibrium points will not only give a basic picture of the phase space, but also pro-

Fig. 1 The spacecraft moving
around a small asteroid
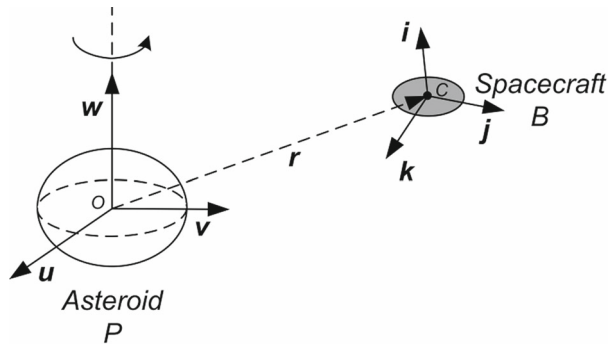
vide potential applications for the asteroid close-proximity operations, such as the asteroid
body-fixed hovering.

2 Statement of problem

As described by Fig. 1, the problem we studied here is the motion of a rigid spacecraft B
around a small asteroid P. Body-fixed reference frames of the asteroid and spacecraft are
given by $S_P = \{u, v, w\}$ and $S_B = \{i, j, k\}$ with O and C as their origins, respectively. The
origin of S_P is fixed at the asteroid mass center, and the coordinate axes are chosen to be
aligned along the principal moments of inertia. The moments of inertia of the asteroid are
assumed to satisfy

$$I_{P,zz} > I_{P,yy}, \quad I_{P,zz} > I_{P,xx}. \tag{1}$$

The second degree and order gravity field of the asteroid can be represented by the har-
monic coefficients C_{20} and C_{22} with other harmonic coefficients vanished, since the origin
of S_P is fixed at the mass center and the coordinate axes are aligned along the principal
moments of inertia. C_{20} and C_{22} can be defined by (Hu and Scheeres 2004)

$$C_{20} = -\frac{1}{2Ma_e^2}\left(2I_{P,zz} - I_{P,xx} - I_{P,yy}\right) < 0, \quad C_{22} = \frac{1}{4Ma_e^2}\left(I_{P,yy} - I_{P,xx}\right), \tag{2}$$

where M and a_e are the asteroid's mass and mean equatorial radius, respectively.

It is assumed that the asteroid is rotating uniformly around its maximum-moment principal
axis, i.e., w-axis, with the angular velocity ω_T. Also S_B is attached to the mass center of the
spacecraft and coincides with the principal axes frame.

The attitude of the spacecraft is described with respect to S_P by A

$$A = \left[\alpha, \beta, \gamma\right]^T, \tag{3}$$

where vectors α, β, and γ are coordinates of u, v, and w expressed in S_B, respectively. A is
also the coordinate transformation matrix from S_B to S_P. The position vector of the spacecraft
with respect to the asteroid mass center O expressed in S_P is given by $r = [x, y, z]^T$.
$\bar{r} = [\bar{x}, \bar{y}, \bar{z}]^T$ is the unit vector along r. The mass of the spacecraft is denoted by m, and the
inertia tensor I is denoted by

$$I = diag\left\{I_{xx}, I_{yy}, I_{zz}\right\}, \tag{4}$$

with the moments of inertia I_{xx}, I_{yy}, and I_{zz}.

3 Equations of motion and perturbations

The equations of orbital motion expressed in the asteroid frame that is uniformly rotating around the maximum-moment principal axis is given by (Scheeres 2012b)

$$\ddot{\boldsymbol{r}} + 2\boldsymbol{\omega}_T \times \dot{\boldsymbol{r}} + \boldsymbol{\omega}_T \times \boldsymbol{\omega}_T \times \boldsymbol{r} = \boldsymbol{\alpha}_{s/c}, \tag{5}$$

where $\boldsymbol{\alpha}_{s/c}$ is the acceleration of the spacecraft and $\boldsymbol{\omega}_T = [0, 0, \omega_T]^T$.

In the attitude-restricted orbital dynamics, the asteroid's non-spherical gravity and GOACP are considered. The perturbations caused by SRP and solar tide are neglected. According to Wang et al. (2014b), $\boldsymbol{\alpha}_{s/c}$ expressed in the asteroid frame can be obtained through a coordinate transformation from S_B to S_P

$$\boldsymbol{\alpha}_{s/c} = \boldsymbol{\alpha}_{Kepler} + \boldsymbol{\alpha}_{NSG} + \boldsymbol{\alpha}_{OAC}. \tag{6}$$

In Eq. (6), $\boldsymbol{\alpha}_{Kepler}$ is the Kepler two-body acceleration

$$\boldsymbol{\alpha}_{Kepler} = -\frac{\mu}{r^2}\bar{\boldsymbol{r}}, \tag{7}$$

where $\mu = GM$, and G is the gravitational constant; $\boldsymbol{\alpha}_{NSG}$ is the perturbation acceleration of the asteroid's non-spherical gravity truncated on the second-order

$$\boldsymbol{\alpha}_{NSG} = \frac{3\mu}{2r^4} \left\{ \left[\tau_0 \left(1 - 5\bar{z}^2 \right) - 10\tau_2 \left(\bar{x}^2 - \bar{y}^2 \right) \right] \bar{\boldsymbol{r}} + 2\tau_0 \bar{z}\boldsymbol{e}_3 + 4\tau_2 \left(\bar{x}\boldsymbol{e}_1 - \bar{y}\boldsymbol{e}_2 \right) \right\}, \tag{8}$$

where $\tau_0 = a_e^2 C_{20}$, $\tau_2 = a_e^2 C_{22}$, $\boldsymbol{e}_1 = [1, 0, 0]^T$, $\boldsymbol{e}_2 = [0, 1, 0]^T$, and $\boldsymbol{e}_3 = [0, 0, 1]^T$; $\boldsymbol{\alpha}_{OAC}$ is the acceleration caused by GOACP truncated on the second-order

$$\boldsymbol{\alpha}_{OAC} = \frac{3\mu}{2r^4} \left\{ \left[5\bar{\boldsymbol{r}}^T A \left(\frac{\boldsymbol{I}}{m} \right) A^T \bar{\boldsymbol{r}} - tr \left(\frac{\boldsymbol{I}}{m} \right) \right] \bar{\boldsymbol{r}} - 2A \left(\frac{\boldsymbol{I}}{m} \right) A^T \bar{\boldsymbol{r}} \right\}. \tag{9}$$

Here it deserves our special attention that, from the viewpoint of two bodies interacting through their mutual gravitational potential, the force model given by Eq. (6) is a second-order approximation of the full gravitational force. That is, $\boldsymbol{\alpha}_{s/c}$ in Eq. (6) contains the zeroth-order term $\boldsymbol{\alpha}_{Kepler}$, caused by the interaction between the zeroth-order mass distributions of the asteroid and spacecraft, i.e., their masses, the second-order term $\boldsymbol{\alpha}_{NSG}$, caused by the interaction between the zeroth-order mass distribution of the spacecraft and the second-order mass distribution of the asteroid, i.e., C_{20} and C_{22}, and the second-order term $\boldsymbol{\alpha}_{OAC}$, caused by the interaction between the zeroth-order mass distribution of the asteroid and the second-order mass distribution of the spacecraft, i.e., the moments of inertia.

Since the first-order mass distribution parameters of the asteroid and spacecraft, i.e., their products of inertia, are all vanished in the principal axes frames S_P and S_B, in $\boldsymbol{\alpha}_{s/c}$, there is not a second-order term caused by the interaction between the first-order mass distributions of the bodies. In $\boldsymbol{\alpha}_{s/c}$, there are not first-order terms either, which, if exist, would be caused by the interaction between the first-order mass distribution of one body and the zeroth-order mass distribution (mass) of the other body.

In the model, GOACP $\boldsymbol{\alpha}_{OAC}$, which is associated with the central gravity term (zeroth-order mass distribution) of the asteroid and the second-order mass distribution of the spacecraft, is the dominant term of the full GOACP. Here, the full GOACP can be defined as the difference of the gravitational force on an extended spacecraft versus that on a point mass spacecraft. Actually, there are higher-order terms of GOACP, which are associated with higher-order gravity terms of the asteroid or higher-order mass distribution parameters of the spacecraft, but their effect is much weaker than that of $\boldsymbol{\alpha}_{OAC}$.

As stated above, from the viewpoint of two bodies interacting through the mutual potential, the non-spherical gravity $\boldsymbol{\alpha}_{NSG}$ and GOACP $\boldsymbol{\alpha}_{OAC}$ are actually both second-order terms. The difference between them is which body is treated as a point mass and which body is treated as an extended body with the second-order mass distribution: in $\boldsymbol{\alpha}_{NSG}$, the spacecraft and asteroid are treated as a point mass and an extended body, respectively, whereas, in $\boldsymbol{\alpha}_{OAC}$, it is the opposite case.

As shown by Eqs. (8) and (9), the ratio of GOACP to the asteroid non-spherical gravity is order of $(\rho/a_e)^2$, determined by the relative dimension of the spacecraft with respect to the asteroid. Usually, ρ is smaller than a_e, therefore in the previous close-proximity orbital dynamics only $\boldsymbol{\alpha}_{NSG}$ is considered and $\boldsymbol{\alpha}_{OAC}$ is neglected. However, as ρ increases, GOACP will increase at the rate of ρ^2. In this paper, as stated before, what we intend is to include $\boldsymbol{\alpha}_{OAC}$ for large spacecraft.

Notice that if SRP and solar tide are considered, because of the asteroid's rotation, the solar position is changing with time in the asteroid body-fixed frame, and the existence of equilibrium points may be much more complicated. In this study, we will focus on the equilibrium points under perturbations of only the non-spherical gravity and GOACP. The effects of SRP and solar tide can be assessed numerically in future studies.

GOACP $\boldsymbol{\alpha}_{OAC}$ depends on the parameter $\boldsymbol{I}/m$ of the spacecraft, which can be described by three parameters: the mass distribution parameters σ_x and σ_y, and the characteristic dimension ρ. σ_x and σ_y are defined as

$$\sigma_x = \left(\frac{I_{zz} - I_{yy}}{I_{xx}} \right), \quad \sigma_y = \left(\frac{I_{zz} - I_{xx}}{I_{yy}} \right), \tag{10}$$

which have the following range

$$-1 \leq \sigma_y \leq 1, \quad -1 \leq \sigma_x \leq 1. \tag{11}$$

Bounds of σ_y and σ_x are determined by the properties of the moments of inertia of a rigid body: $I_{xx} + I_{yy} > I_{zz}$, $I_{xx} + I_{zz} > I_{yy}$, and $I_{yy} + I_{zz} > I_{xx}$.

The characteristic dimension ρ, which is an estimation but not the real value, is defined by (Wang et al. 2014a)

$$\frac{1}{2}\rho^2 = \frac{I_{xx}}{m}. \tag{12}$$

As shown above, I_{xx}/m describes the spacecraft characteristic dimension, and σ_x and σ_y describe its non-spherical mass distribution. These are two basic elements of the gravitational orbit–attitude coupling, which will be more significant with a larger ratio of the characteristic dimension to the orbital radius or with a more non-spherical mass distribution.

4 Equilibrium points

Equilibrium points means that the spacecraft is staying stationary in the asteroid body-fixed frame. That is to say, the spacecraft is on a stationary orbit. Since the asteroid is rotating uniformly around its $\boldsymbol{w}$-axis, the trajectory of the spacecraft in the inertial space is a circle perpendicular to the asteroid's rotational axis.

4.1 Equilibrium and stability conditions

4.1.1 Equilibrium conditions

Equilibrium conditions can be easily obtained by setting $\ddot{\boldsymbol{r}} = \boldsymbol{0}$ and $\dot{\boldsymbol{r}} = \boldsymbol{0}$ in the equations of motion (5)

$$\boldsymbol{\omega}_T \times \boldsymbol{\omega}_T \times \boldsymbol{r} = \boldsymbol{\alpha}_{s/c}, \tag{13}$$

which actually means that the gravitational force acting on the spacecraft balances the centrifugal force of the circular orbital motion. By using Eqs. (6)–(9), the equilibrium condition (13) can be written as

$$\boldsymbol{\omega}_T \times \boldsymbol{\omega}_T \times \boldsymbol{r} = -\frac{\mu}{r^2}\bar{\boldsymbol{r}} + \frac{3\mu}{2r^4}\left\{[\tau_0\left(1 - 5\bar{z}^2\right) - 10\tau_2\left(\bar{x}^2 - \bar{y}^2\right)]\bar{\boldsymbol{r}} + 2\tau_0\bar{z}\boldsymbol{e}_3 + 4\tau_2\left(\bar{x}\boldsymbol{e}_1 - \bar{y}\boldsymbol{e}_2\right)\right\}$$
$$+ \frac{3\mu}{2r^4}\left\{\left[5\bar{\boldsymbol{r}}^T A\left(\frac{\boldsymbol{I}}{m}\right)A^T\bar{\boldsymbol{r}} - \mathrm{tr}\left(\frac{\boldsymbol{I}}{m}\right)\right]\bar{\boldsymbol{r}} - 2A\left(\frac{\boldsymbol{I}}{m}\right)A^T\bar{\boldsymbol{r}}\right\}. \tag{14}$$

4.1.2 Stability conditions

The stability of equilibrium points is an important qualitative property. To study the stability, we need to linearize the orbital dynamics Eq. (5) at the equilibrium point $\boldsymbol{r}_e$. Equation (5) can be rewritten as

$$\frac{d}{dt}\begin{bmatrix} \dot{\boldsymbol{r}} \\ \boldsymbol{r} \end{bmatrix} = \begin{bmatrix} -2\omega_T\hat{\boldsymbol{e}}_3 & -\omega_T^2\hat{\boldsymbol{e}}_3\hat{\boldsymbol{e}}_3 \\ \boldsymbol{E} & \boldsymbol{0} \end{bmatrix}\begin{bmatrix} \dot{\boldsymbol{r}} \\ \boldsymbol{r} \end{bmatrix} + \begin{bmatrix} \boldsymbol{\alpha}_{s/c} \\ \boldsymbol{0} \end{bmatrix}, \tag{15}$$

where $\boldsymbol{E}$ is the 3×3 identity matrix, and the hat map $\wedge$ is

$$\hat{\boldsymbol{e}}_3 = \begin{bmatrix} 0 & -1 & 0 \\ 1 & 0 & 0 \\ 0 & 0 & 0 \end{bmatrix}. \tag{16}$$

$\dot{\boldsymbol{r}}$ and $\boldsymbol{r}$ can be written in terms of variations $\delta\dot{\boldsymbol{r}}$ and $\delta\boldsymbol{r}$ as

$$\dot{\boldsymbol{r}} = \boldsymbol{0} + \delta\dot{\boldsymbol{r}}, \quad \boldsymbol{r} = \boldsymbol{r}_e + \delta\boldsymbol{r}. \tag{17}$$

Then, the linearized equation near $\boldsymbol{r}_e$ is given by

$$\frac{d}{dt}\begin{bmatrix} \boldsymbol{0} + \delta\dot{\boldsymbol{r}} \\ \boldsymbol{r}_e + \delta\boldsymbol{r} \end{bmatrix} = \begin{bmatrix} -2\omega_T\hat{\boldsymbol{e}}_3 & -\omega_T^2\hat{\boldsymbol{e}}_3\hat{\boldsymbol{e}}_3 \\ \boldsymbol{E} & \boldsymbol{0} \end{bmatrix}\begin{bmatrix} \boldsymbol{0} + \delta\dot{\boldsymbol{r}} \\ \boldsymbol{r}_e + \delta\boldsymbol{r} \end{bmatrix} + \begin{bmatrix} \boldsymbol{\alpha}_{s/c}\big|_e + \frac{\partial\boldsymbol{\alpha}_{s/c}}{\partial\boldsymbol{r}}\bigg|_e \delta\boldsymbol{r} \\ \boldsymbol{0} \end{bmatrix}. \tag{18}$$

According to equilibrium conditions at $\boldsymbol{r}_e$

$$\begin{bmatrix} \boldsymbol{0} \\ \boldsymbol{0} \end{bmatrix} = \begin{bmatrix} -2\omega_T\hat{\boldsymbol{e}}_3 & -\omega_T^2\hat{\boldsymbol{e}}_3\hat{\boldsymbol{e}}_3 \\ \boldsymbol{E} & \boldsymbol{0} \end{bmatrix}\begin{bmatrix} \boldsymbol{0} \\ \boldsymbol{r}_e \end{bmatrix} + \begin{bmatrix} \boldsymbol{\alpha}_{s/c}\big|_e \\ \boldsymbol{0} \end{bmatrix}, \tag{19}$$

the variation equation near $\boldsymbol{r}_e$ can be obtained

$$\frac{d}{dt}\begin{bmatrix} \delta\dot{\boldsymbol{r}} \\ \delta\boldsymbol{r} \end{bmatrix} = \begin{bmatrix} -2\omega_T\hat{\boldsymbol{e}}_3 & -\omega_T^2\hat{\boldsymbol{e}}_3\hat{\boldsymbol{e}}_3 + \frac{\partial\boldsymbol{\alpha}_{s/c}}{\partial\boldsymbol{r}}\bigg|_e \\ \boldsymbol{E} & \boldsymbol{0} \end{bmatrix}\begin{bmatrix} \delta\dot{\boldsymbol{r}} \\ \delta\boldsymbol{r} \end{bmatrix}. \tag{20}$$

The linear stability is determined by the system matrix of the linearized system

$$D\left(r_e\right) = \begin{bmatrix} -2\omega_T \hat{e}_3 & -\omega_T^2 \hat{e}_3 \hat{e}_3 + \left.\frac{\partial \boldsymbol{\alpha}_{s/c}}{\partial r}\right|_e \\ \mathbf{E} & 0 \end{bmatrix}, \tag{21}$$

all the eigenvalues of which are required to have a non-positive real part for the linear stability. Since the system is conservative, there is only even terms in the characteristic polynomial of $D(r_e)$, and the eigenvalues will be symmetrical with respect to both the real and imaginary axes. Then, the linear stability requires all the eigenvalues of $D(r_e)$ to be purely imaginary.

Notice that $D(r_e)$ is determined by the angular velocity ω_T and the gradient of $\boldsymbol{\alpha}_{s/c}$. According to Eqs. (6)–(9), the gradient of $\boldsymbol{\alpha}_{s/c}$ can be derived as

$$\begin{aligned}
\frac{\partial \boldsymbol{\alpha}_{s/c}}{\partial r} =\ & -\frac{\mu}{r^3}\left(\mathbf{E} - 3\bar{r}\bar{r}^T\right) \\
& -\frac{3\mu}{2r^5}\left\{5\bar{r}^T A\left(\frac{I}{m}\right)A^T\bar{r} - tr\left(\frac{I}{m}\right) + \tau_0\left(1 - 5\bar{z}^2\right) - 10\tau_2\left(\bar{x}^2 - \bar{y}^2\right)\right\}\left\{7\bar{r}\bar{r}^T - \mathbf{E}\right\} \\
& -\frac{3\mu}{r^5}\left\{\left[tr\left(\frac{I}{m}\right) - \tau_0\right]\bar{r}\bar{r}^T + A\left(\frac{I}{m}\right)A^T - \tau_0 e_3 e_3^T - 2\tau_2\left(e_1 e_1^T - e_2 e_2^T\right)\right\} \\
& -\frac{15\mu}{r^5}\left\{-A\left(\frac{I}{m}\right)A^T\bar{r}\bar{r}^T - \bar{r}\bar{r}^T A\left(\frac{I}{m}\right)A^T + \tau_0\bar{z}\left(e_3\bar{r}^T + \bar{r}e_3^T\right)\right. \\
& \left. + 2\tau_2\left[\bar{x}\left(e_1\bar{r}^T + \bar{r}e_1^T\right) - \bar{y}\left(e_2\bar{r}^T + \bar{r}e_2^T\right)\right]\right\}.
\end{aligned} \tag{22}$$

We can see that the formula of $\frac{\partial \boldsymbol{\alpha}_{s/c}}{\partial r}$ is tedious and it is difficult to obtain the explicit formula of the characteristic polynomial of $D(r_e)$. The stability depends on not only the asteroid parameters: μ, ω_T, τ_0, and τ_2, but also the spacecraft parameters: A, I, and m.

In the calculation of off-axis equilibrium points, we will determine the stability by numerical calculations and give some discussions. It will need lots of work to investigate the stability thoroughly with respect to all the system parameters. The stability analysis of the six degree-of-freedom rigid body motion has been carried out in several previous works, such as Wang et al. (1991, 1992, 2014b), Wang and Xu (2013d). A similar method can be used in the stability analysis of this problem. However, should keep in mind that in this problem the three degree-of-freedom translational motion is studied, but not the six degree-of-freedom rigid body motion.

4.2 Previous results

In previous studies on the close-proximity orbital dynamics about asteroids, such as Hu (2002), only the perturbation acceleration of the asteroid's non-spherical gravity was considered, i.e., $\boldsymbol{\alpha}_{s/c} = \boldsymbol{\alpha}_{Kepler} + \boldsymbol{\alpha}_{NSG}$. Then, the equilibrium condition is

$$\begin{aligned}
& \boldsymbol{\omega}_T \times \boldsymbol{\omega}_T \times r \\
& = -\frac{\mu}{r^2}\bar{r} + \frac{3\mu}{2r^4}\left\{\left[\tau_0\left(1 - 5\bar{z}^2\right) - 10\tau_2\left(\bar{x}^2 - \bar{y}^2\right)\right]\bar{r} + 2\tau_0\bar{z}e_3 + 4\tau_2\left(\bar{x}e_1 - \bar{y}e_2\right)\right\}. \tag{23}
\end{aligned}$$

Previous results based on Eq. (23) have shown that within the equatorial plane of the asteroid there exist two kinds of equilibrium points, which lie on the u-axes and on the v-axis. It is impossible to have equilibrium points at other longitudes.

The radii of these stationary orbits on the $\boldsymbol{u}$- and $\boldsymbol{v}$-axes satisfy the following equations, respectively

$$\omega_T^2 r = \frac{\mu}{r^2} - \frac{3\mu}{2r^4} \left(\tau_0 - 6\tau_2\right), \tag{24}$$

$$\omega_T^2 r = \frac{\mu}{r^2} - \frac{3\mu}{2r^4} \left(\tau_0 + 6\tau_2\right). \tag{25}$$

The stationary orbits lying on the longer-axis ($\boldsymbol{u}$-axis) are always unstable, while those lying on the shorter-axis ($\boldsymbol{v}$-axis) are stable under the following approximated condition (Hu 2002)

$$\left(\frac{\mu}{\omega_T^2}\right)^{2/3} + \tau_0 - 162\tau_2 > 0. \tag{26}$$

4.3 Equilibrium points within equatorial plane

Because of GOACP $\boldsymbol{\alpha}_{OAC}$, the equilibrium points determined by Eq. (14) in the attitude-restricted orbital dynamics will be different from the previous classical equilibrium points without $\boldsymbol{\alpha}_{OAC}$ determined by Eq. (23).

GOACP $\boldsymbol{\alpha}_{OAC}$ introduces several new parameters into the system, including the spacecraft attitude $\boldsymbol{A}$ and parameter $\boldsymbol{I}/m$, which includes σ_x, σ_y, and ρ. The system is more complicated than the previous classical system Eq. (23), and the types and locations of equilibrium points will be more diverse.

In the present paper, we will study the equilibrium points within the asteroid equatorial plane, that is $\bar{z} = 0$ in the equilibrium condition (14). Then, we can have the new equilibrium condition within the equatorial plane as

$$\omega_T^2 r = \frac{\mu}{r^2}\bar{\boldsymbol{r}} - \frac{3\mu}{2r^4} \left\{ \left[\tau_0 - 10\tau_2 \left(\bar{x}^2 - \bar{y}^2\right) + 5\bar{\boldsymbol{r}}^T \boldsymbol{A}\left(\boldsymbol{I}/m\right)\boldsymbol{A}^T\bar{\boldsymbol{r}} - tr(\boldsymbol{I}/m)\right]\bar{\boldsymbol{r}} \right.$$
$$\left. + 4\tau_2 \left(\bar{x}\boldsymbol{e}_1 - \bar{y}\boldsymbol{e}_2\right) - 2\boldsymbol{A}\left(\boldsymbol{I}/m\right)\boldsymbol{A}^T\bar{\boldsymbol{r}} \right\}, \tag{27}$$

which requires that $4\tau_2(\bar{x}\boldsymbol{e}_1 - \bar{y}\boldsymbol{e}_2) - 2\boldsymbol{A}(\boldsymbol{I}/m)\boldsymbol{A}^T\bar{\boldsymbol{r}}$ is parallel to the position vector $\bar{\boldsymbol{r}}$.

4.4 On-axis equilibrium points

First we focus on the on-axis equilibrium points. We assume that the equilibrium point is located on the equatorial principal axes, i.e., on the $\boldsymbol{u}$- or $\boldsymbol{v}$-axis.

4.4.1 On $\boldsymbol{u}$-axis

If the spacecraft is located on the $\boldsymbol{u}$-axis, we have $\bar{x} = \pm 1$, $\bar{y} = 0$, and $\bar{\boldsymbol{r}} = [\pm 1, 0, 0] = \pm\boldsymbol{e}_1$ in Eq. (27), and then the new equilibrium condition is given by

$$\omega_T^2 r \boldsymbol{e}_1 = \frac{\mu}{r^2}\boldsymbol{e}_1 - \frac{3\mu}{2r^4} \left\{ \left[\tau_0 - 6\tau_2 + 5\boldsymbol{e}_1^T \boldsymbol{A}(\boldsymbol{I}/m)\boldsymbol{A}^T\boldsymbol{e}_1 - tr(\boldsymbol{I}/m)\right]\boldsymbol{e}_1 - 2\boldsymbol{A}(\boldsymbol{I}/m)\boldsymbol{A}^T\boldsymbol{e}_1 \right\}. \tag{28}$$

This requires that $\boldsymbol{e}_1$ is the eigenvector of the matrix $\boldsymbol{A}(\boldsymbol{I}/m)\boldsymbol{A}^T$, which is actually the inertia tensor of the spacecraft expressed in the asteroid frame S_P. That is to say, the $\boldsymbol{u}$-axis of the asteroid lies on the principal axis of the spacecraft.

Without loss of generality, we assume that the $\boldsymbol{u}$-axis lies on the $\boldsymbol{i}$-axis of the spacecraft and have the same positive direction. Other cases can be converted into this case by changing the arrangement of axes of the spacecraft's body frame. In this case, the relative attitude of the spacecraft with respect to the asteroid is just a single axis rotation around the $\boldsymbol{u}$-axis, i.e.,

$$A = \begin{bmatrix} 1 & 0 & 0 \\ 0 & \cos\phi & -\sin\phi \\ 0 & \sin\phi & \cos\phi \end{bmatrix}, \tag{29}$$

where ϕ is the rotational angle. Therefore, we have

$$A(I/m)A^T = \begin{bmatrix} I_{xx}/m & 0 & 0 \\ 0 & \cos^2\phi I_{yy}/m + \sin^2\phi I_{zz}/m & \sin\phi\cos\phi\left(I_{yy}/m - I_{zz}/m\right) \\ 0 & \sin\phi\cos\phi\left(I_{yy}/m - I_{zz}/m\right) & \sin^2\phi I_{yy}/m + \cos^2\phi I_{zz}/m \end{bmatrix}. \tag{30}$$

Then, the equilibrium condition (28) can be written as

$$\omega_T^2 r = \frac{\mu}{r^2} - \frac{3\mu}{2r^4}\left[2\frac{I_{xx}}{m} - \frac{I_{yy}}{m} - \frac{I_{zz}}{m} + \tau_0 - 6\tau_2\right]. \tag{31}$$

The orbital radius of the equilibrium point, which is the same with the orbital radius of the relative equilibrium in the gravitationally coupled orbit–attitude (full) dynamics (Wang et al. 2014b; Wang and Xu 2014b), will be determined by Eq. (31). At the relative equilibrium in Wang et al. (2014b), the spacecraft has the same attitude with the asteroid, i.e., $\phi = 0$. Here, the rotational angle ϕ does not affect the location of the equilibrium point. This is because in the orbital dynamics Eq. (5) the gravitational force has been truncated up to the second order, and at the equilibrium point the rotational angle ϕ only affects the higher-order terms.

Through the comparison between Eqs. (24) and (31), we can easily see the effect of GOACP $\boldsymbol{\alpha}_{OAC}$. Different from the previous orbital dynamics without $\boldsymbol{\alpha}_{OAC}$ in Eq. (24), the orbital motion of the spacecraft in Eq. (31) is affected by its moments of inertia. This effect can be considered as an equivalent change of the oblateness and ellipticity of the asteroid from the viewpoint of orbital dynamics without $\boldsymbol{\alpha}_{OAC}$. Notice that in the case of $I_{xx} = I_{yy} = I_{zz}$, i.e., the spacecraft is a homogeneous sphere under the second-order approximation, the effects of moments of inertia are vanished. In this case, Eq. (31) will be reduced to the previous result without $\boldsymbol{\alpha}_{OAC}$ in Eq. (24). Besides, for a larger ρ, GOACP is more significant. These results are consistent with the physical origin of the gravitational orbit–attitude coupling.

Because of the symmetry, if the $\boldsymbol{u}$-axis lies on the $\boldsymbol{i}$-axis of spacecraft but has the opposite direction, we can also have the orbital radius given by Eq. (31).

If the $\boldsymbol{u}$-axes lies on the $\boldsymbol{j}$- and $\boldsymbol{k}$-axes of the spacecraft, with the same method, we can obtain the similar equilibrium conditions, respectively

$$\omega_T^2 r = \frac{\mu}{r^2} - \frac{3\mu}{2r^4}\left[2\frac{I_{yy}}{m} - \frac{I_{xx}}{m} - \frac{I_{zz}}{m} + \tau_0 - 6\tau_2\right], \tag{32}$$

$$\omega_T^2 r = \frac{\mu}{r^2} - \frac{3\mu}{2r^4}\left[2\frac{I_{zz}}{m} - \frac{I_{xx}}{m} - \frac{I_{yy}}{m} + \tau_0 - 6\tau_2\right]. \tag{33}$$

4.4.2 On $\boldsymbol{v}$-axis

If we assume that the spacecraft is located on the $\boldsymbol{v}$-axis, we will have $\bar{x} = 0$, $\bar{y} = \pm 1$, and $\bar{\boldsymbol{r}} = [0, \pm 1, 0] = \pm \boldsymbol{e}_2$ in the equilibrium condition (27), and then the corresponding new equilibrium condition is given by

$$\omega_T^2 r e_2 = \frac{\mu}{r^2} e_2 - \frac{3\mu}{2r^4} \left\{ \left[\tau_0 + 6\tau_2 + 5e_2^T A(I/m)A^T e_2 - tr(I/m) \right] e_2 - 2A(I/m)A^T e_2 \right\}. \tag{34}$$

This requires that e_2 is the eigenvector of $A(I/m)A^T$. That is to say, the v-axis of the asteroid lies on the principal axis of the spacecraft.

With a similar method with the cases on the u-axis, we can obtain the equations determining the orbital radius of equilibrium points as

$$\omega_T^2 r = \frac{\mu}{r^2} - \frac{3\mu}{2r^4} \left[2\frac{I_{xx}}{m} - \frac{I_{yy}}{m} - \frac{I_{zz}}{m} + \tau_0 + 6\tau_2 \right], \tag{35}$$

$$\omega_T^2 r = \frac{\mu}{r^2} - \frac{3\mu}{2r^4} \left[2\frac{I_{yy}}{m} - \frac{I_{xx}}{m} - \frac{I_{zz}}{m} + \tau_0 + 6\tau_2 \right], \tag{36}$$

$$\omega_T^2 r = \frac{\mu}{r^2} - \frac{3\mu}{2r^4} \left[2\frac{I_{zz}}{m} - \frac{I_{xx}}{m} - \frac{I_{yy}}{m} + \tau_0 + 6\tau_2 \right], \tag{37}$$

which correspond to the cases that the v-axis lies on the i-, j-, and k-axes of the spacecraft, respectively. The differences between Eqs. (35)–(37) and the previous orbital dynamics Eq. (25) are due to GOACP α_{OAC}.

As stated above, the on-axis equilibrium points can be divided into four groups, which are on the $+u$-, $-u$-, $+v$-, and $-v$-axes of the asteroid, respectively. In each group, there exist three different cases that the equatorial principal axis of the asteroid lies on the i-, j-, and k-axes of the spacecraft, respectively. Although the longitudes of equilibrium points are the same with those in the previous orbital dynamics without α_{OAC}, the orbital radii are different due to GOACP α_{OAC}, as shown by Eqs. (31)–(33) and (35)–(37).

4.5 Off-axis equilibrium points

In this subsection, we obtain the off-axis equilibrium points, which are located off the u- and v-axes of the asteroid. These off-axis equilibrium points cannot exist in the previous orbital dynamics without α_{OAC}, but can exist in the attitude-restricted orbital dynamics due to GOACP.

The spacecraft can stay at a stable equilibrium point without orbital control, and stay at an unstable equilibrium point with small orbital control without needing to null out the unbalanced gravity. Therefore, the off-axis equilibrium points can be useful in the asteroid close-proximity operations, such as the asteroid body-fixed hovering.

4.5.1 Off-axis equilibrium conditions

As for these off-axis equilibrium points, we have $\bar{x} \neq 0$, $\bar{y} \neq 0$, and $\bar{r} = [\bar{x}, \bar{y}, 0]$ in the equilibrium condition (27), which cannot be simplified further.

Equation (27) requires that $4\tau_2(\bar{x}e_1 - \bar{y}e_2) - 2A(I/m)A^T\bar{r}$ is parallel to $\bar{r}$. Notice that $\bar{r}$ is within the equatorial plane spanned by e_1 and e_2, therefore $A(I/m)A^T\bar{r}$ should also be within the equatorial plane. Then, we can know that the equatorial plane is the principal plane of the inertia tensor $A(I/m)A^T$ that is expressed in S_P. That is to say, one of the i–j plane, j–k plane, and i–k plane of the spacecraft is within the e_1–e_2 plane of the asteroid. Without loss of generality, we assume that the i–j plane is within the e_1–e_2 plane, and the unit normal vector k of the i–j plane has the same direction with e_3. Other cases can be converted into this case by changing the arrangement of axes of S_B. That is to say, the relative attitude of the spacecraft with respect to the asteroid is just a single axis rotation around the w-axis, i.e.,

$$A = \begin{bmatrix} \cos\psi & -\sin\psi & 0 \\ \sin\psi & \cos\psi & 0 \\ 0 & 0 & 1 \end{bmatrix}, \tag{38}$$

where ψ is the rotational angle. Therefore, we have

$$A(I/m)A^T = \begin{bmatrix} \cos^2\psi\, I_{xx}/m + \sin^2\psi\, I_{yy}/m & \sin\psi\cos\psi\left(I_{xx}/m - I_{yy}/m\right) & 0 \\ \sin\psi\cos\psi\left(I_{xx}/m - I_{yy}/m\right) & \sin^2\psi\, I_{xx}/m + \cos^2\psi\, I_{yy}/m & 0 \\ 0 & 0 & I_{zz}/m \end{bmatrix}, \tag{39}$$

$$\begin{aligned}
4\tau_2\left(\bar{x}\boldsymbol{e}_1 - \bar{y}\boldsymbol{e}_2\right) - 2A(I/m)A^T\bar{\boldsymbol{r}} \\
= 2\begin{bmatrix} -\left(\cos^2\psi\, I_{xx}/m + \sin^2\psi\, I_{yy}/m - 2\tau_2\right)\bar{x} - \sin\psi\cos\psi\left(I_{xx}/m - I_{yy}/m\right)\bar{y} \\ -\sin\psi\cos\psi\left(I_{xx}/m - I_{yy}/m\right)\bar{x} - \left(\sin^2\psi\, I_{xx}/m + \cos^2\psi\, I_{yy}/m + 2\tau_2\right)\bar{y} \\ 0 \end{bmatrix}.
\end{aligned} \tag{40}$$

Then, the condition that $4\tau_2(\bar{x}\boldsymbol{e}_1 - \bar{y}\boldsymbol{e}_2) - 2A(I/m)A^T\bar{\boldsymbol{r}}$ is parallel to $\bar{\boldsymbol{r}}$ is equivalent to

$$\frac{\left(\cos^2\psi\, I_{xx}/m + \sin^2\psi\, I_{yy}/m - 2\tau_2\right)\bar{x} + \sin\psi\cos\psi\left(I_{xx}/m - I_{yy}/m\right)\bar{y}}{\sin\psi\cos\psi\left(I_{xx}/m - I_{yy}/m\right)\bar{x} + \left(\sin^2\psi\, I_{xx}/m + \cos^2\psi\, I_{yy}/m + 2\tau_2\right)\bar{y}} = \frac{\bar{x}}{\bar{y}}, \tag{41}$$

which can be further simplified as

$$\frac{\left(\cos^2\psi + \sin^2\psi\, I_{yy}/I_{xx} - 4\tau_2/\rho^2\right)\bar{x} + \sin\psi\cos\psi\left(1 - I_{yy}/I_{xx}\right)\bar{y}}{\sin\psi\cos\psi\left(1 - I_{yy}/I_{xx}\right)\bar{x} + \left(\sin^2\psi + \cos^2\psi\, I_{yy}/I_{xx} + 4\tau_2/\rho^2\right)\bar{y}} = \frac{\bar{x}}{\bar{y}}. \tag{42}$$

We can see that the condition (42) is affected by the mass distribution parameter I_{yy}/I_{xx}, the characteristic dimension ρ and the attitude angle ψ of the spacecraft. These parameters are all introduced into the system by GOACP $\boldsymbol{\alpha}_{OAC}$. If $\boldsymbol{\alpha}_{OAC}$ is neglected, Eq. (41) will be $\bar{x}/\bar{y} = -\bar{x}/\bar{y}$, which implies that $\bar{x} = 0$ or $\bar{y} = 0$. This is the reason why the off-axis equilibrium point cannot exist in the previous orbital dynamics without $\boldsymbol{\alpha}_{OAC}$.

After some rearrangements, Eq. (42) can be simplified as

$$\begin{aligned}
\sin\psi\cos\psi\left(1 - I_{yy}/I_{xx}\right)\left(\bar{x}^2 - \bar{y}^2\right) \\
+ \left[\left(\sin^2\psi - \cos^2\psi\right)\left(1 - I_{yy}/I_{xx}\right) + 8C_{22}a_e^2/\rho^2\right]\bar{x}\bar{y} = 0.
\end{aligned} \tag{43}$$

By using the relation $\bar{x}^2 + \bar{y}^2 = 1$, Eq. (43) can be written further as

$$\bar{x}^4 - \bar{x}^2 + c = 0, \tag{44}$$

where

$$c = \frac{\sin^2\psi\cos^2\psi\left(1 - I_{yy}/I_{xx}\right)^2}{4\sin\psi^2\cos\psi^2\left(1 - I_{yy}/I_{xx}\right)^2 + \left[\left(\sin^2\psi - \cos^2\psi\right)\left(1 - I_{yy}/I_{xx}\right) + 8C_{22}a_e^2/\rho^2\right]^2} > 0. \tag{45}$$

Therefore, we have

$$\bar{x}^2 = \frac{1 \pm \sqrt{1 - 4c}}{2}, \tag{46}$$

which contains four solutions: if the terms $\sin \psi \cos \psi (1 - I_{yy}/I_{xx})$ and $(\sin^2 \psi - \cos^2 \psi) \times (1 - I_{yy}/I_{xx}) + 8C_{22}a_e^2/\rho^2$ in Eq. (43) have the same sign, $\bar{x}^2 - \bar{y}^2$ and $\bar{x}\bar{y}$ will have the opposite signs, and then

$$
\begin{aligned}
&(1) \ \bar{x} = \sqrt{\frac{1 + \sqrt{1 - 4c}}{2}}, \quad \bar{y} = -\sqrt{\frac{1 - \sqrt{1 - 4c}}{2}}; \\
&(2) \ \bar{x} = -\sqrt{\frac{1 + \sqrt{1 - 4c}}{2}}, \quad \bar{y} = \sqrt{\frac{1 - \sqrt{1 - 4c}}{2}}; \\
&(3) \ \bar{x} = \sqrt{\frac{1 - \sqrt{1 - 4c}}{2}}, \quad \bar{y} = \sqrt{\frac{1 + \sqrt{1 - 4c}}{2}}; \\
&(4) \ \bar{x} = -\sqrt{\frac{1 - \sqrt{1 - 4c}}{2}}, \quad \bar{y} = -\sqrt{\frac{1 + \sqrt{1 - 4c}}{2}};
\end{aligned}
\tag{47}
$$

If the terms $\sin \psi \cos \psi (1 - I_{yy}/I_{xx})$ and $(\sin^2 \psi - \cos^2 \psi)(1 - I_{yy}/I_{xx}) + 8C_{22}a_e^2/\rho^2$ in Eq. (43) have the opposite signs, $\bar{x}^2 - \bar{y}^2$ and $\bar{x}\bar{y}$ will have the same sign, and then

$$
\begin{aligned}
&(1) \ \bar{x} = \sqrt{\frac{1 + \sqrt{1 - 4c}}{2}}, \quad \bar{y} = \sqrt{\frac{1 - \sqrt{1 - 4c}}{2}}; \\
&(2) \ \bar{x} = -\sqrt{\frac{1 + \sqrt{1 - 4c}}{2}}, \quad \bar{y} = -\sqrt{\frac{1 - \sqrt{1 - 4c}}{2}}; \\
&(3) \ \bar{x} = \sqrt{\frac{1 - \sqrt{1 - 4c}}{2}}, \quad \bar{y} = -\sqrt{\frac{1 + \sqrt{1 - 4c}}{2}}; \\
&(4) \ \bar{x} = -\sqrt{\frac{1 - \sqrt{1 - 4c}}{2}}, \quad \bar{y} = \sqrt{\frac{1 + \sqrt{1 - 4c}}{2}}.
\end{aligned}
\tag{48}
$$

These four solutions are located in four quadrants of the equatorial plane of the asteroid, i.e., the $e_1 - e_2$ plane, respectively. Because of the symmetry of the system, the equilibrium points in the first and third quadrants are symmetrical with respect to the asteroid center, and also the equilibrium points in the second and fourth quadrants. That is, in Eqs. (47) and (48) the first and second solutions have the opposite signs, and also the third and fourth solutions.

With Eqs. (45), (47), and (48), we can obtain the position vector $\bar{r} = [\bar{x}, \bar{y}, 0]$, i.e., the longitude of the off-axis equilibrium point. Then according to Eq. (27), the orbit radius of the off-axis equilibrium point can be calculated by

$$
\omega_T^2 r = \frac{\mu}{r^2} - \frac{3\mu}{2r^4} \left[\tau_0 - 10\tau_2 \left(\bar{x}^2 - \bar{y}^2 \right) + 5\bar{r}^T A(I/m)A^T \bar{r} - tr(I/m) + a \right], \tag{49}
$$

where $a\bar{r} = 4\tau_2(\bar{x}e_1 - \bar{y}e_2) - 2A(I/m)A^T \bar{r}$.

4.5.2 Calculation examples

We want to give some calculation examples of the off-axis equilibrium points and to investigate the effect of GOACP α_{OAC}.

The parameters of the asteroid are chosen to be

$$\mu = 5\,\mathrm{m}^3/\mathrm{s}^2, \quad C_{20} = -0.12, \quad C_{22} = 0.01, \quad a_e = 250\,\mathrm{m}, \quad \omega_T = 2.9089 \times 10^{-4}\,\mathrm{s}^{-1}, \tag{50}$$

which has a similar size with the target of the OSIRIS-REx mission, the asteroid 101955 Bennu (provisional designation 1999 RQ_{36}), but has larger values for C_{20} and C_{22} than the approximate values of Bennu, which are calculated under the assumption of filling its currently best determined shape model with a homogeneous bulk density. The period of the asteroid's uniform rotation is 6 h.

The mass distribution of the spacecraft is set to be

$$I_{xx}:I_{yy}:I_{zz} = 1.5:1:1.2, \tag{51}$$

which is a common case in space engineering. As for ρ, we choose six different values

$$\rho = 2\,\mathrm{m}, \quad \rho = 50\,\mathrm{m}, \quad \rho = 100\,\mathrm{m}, \quad \rho = 120\,\mathrm{m}, \quad \rho = 140\,\mathrm{m}, \quad \rho = 160\,\mathrm{m}. \tag{52}$$

The minimum $\rho = 2$ m corresponds to a general asteroid explorer, such as NEAR mission, OSIRIS-REx mission, and Hayabusa mission. The maximum $\rho = 160$ m corresponds to a much larger spacecraft or a space station in future asteroid deflection missions, such as a big gravity tractor, or the mother ship in the asteroid resource exploitation. These situations are extreme from the viewpoint of current deep space missions, but perhaps will be common in future asteroid missions.

By using Eqs. (47)–(49), the longitudes and orbital radii of off-axis equilibrium points can be calculated. We then plot the locus of equilibrium points in the equatorial plane of the asteroid with respect to the attitude angle ψ in six cases of different ρ. The considered range of ψ is $0 \le \psi \le \pi$, since $\pi \le \psi \le 2\pi$ is actually the same case with $0 \le \psi \le \pi$ because of the symmetry of the spacecraft inertia tensor. The stability of these off-axis equilibrium points are also calculated by using $\boldsymbol{D}(\boldsymbol{r}_e)$ in Eq. (21).

The loci of equilibrium points in the $\boldsymbol{u}-\boldsymbol{v}$ plane in the six cases with respect to $0 \le \psi \le \pi$ are given in Figs. 2, 3, 4, 5, 6, and 7, respectively. In the loci, the stable equilibrium points are denoted by larger dots than the unstable ones. To distinguish between stable and unstable points better, we also indicate the stability using texts in the figures.

Fig. 2 Loci of off-axis equilibrium points with respect to ψ in the case of $\rho = 2$ m
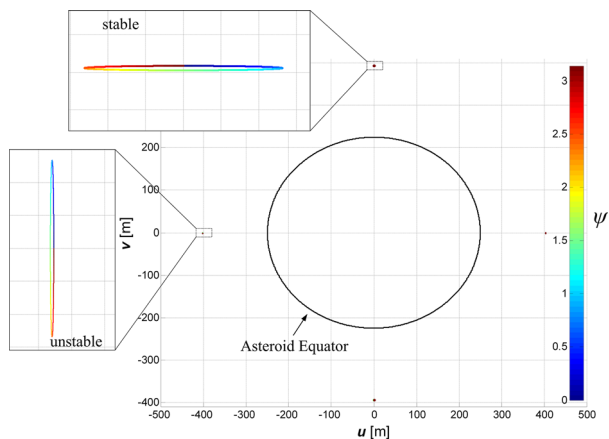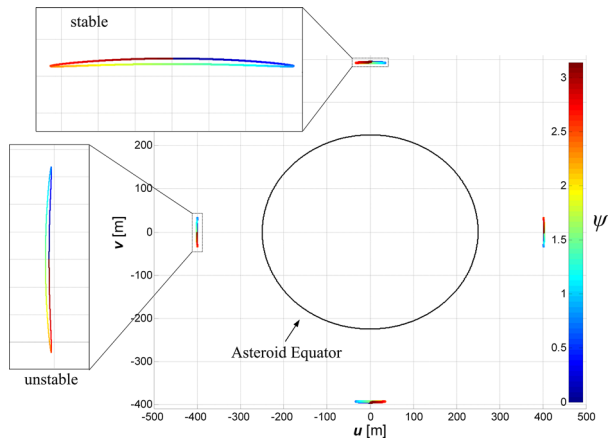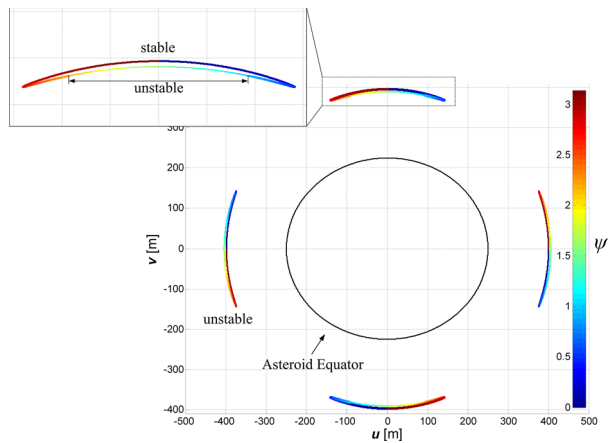
Fig. 3 Loci of off-axis equilibrium points with respect to ψ in the case of $\rho = 50$ m

Fig. 4 Loci of off-axis equilibrium points with respect to ψ in the case of $\rho = 100$ m

Fig. 5 Loci of off-axis equilibrium points with respect to ψ in the case of $\rho = 120$ m
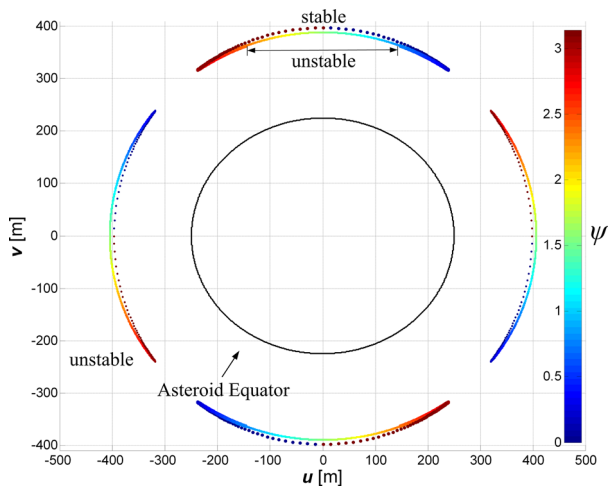
Fig. 6 Loci of off-axis
equilibrium points with respect to
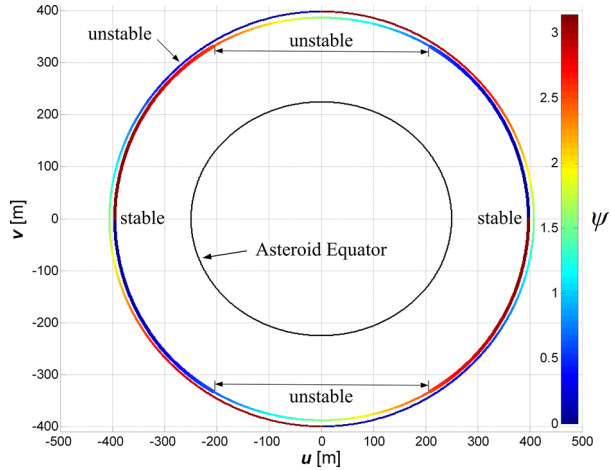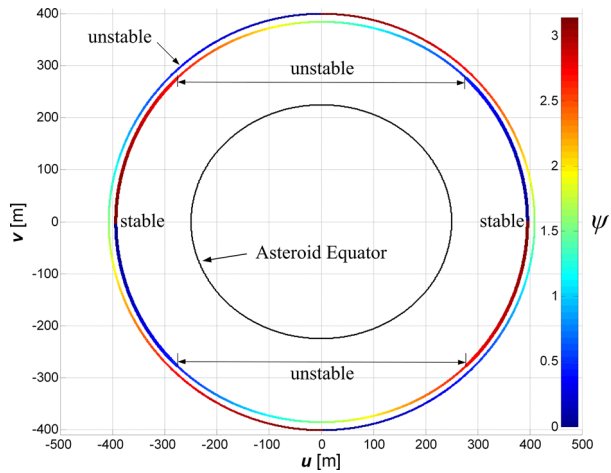ψ in the case of $\rho = 140$ m

Fig. 7 Loci of off-axis
equilibrium points with respect to
ψ in the case of $\rho = 160$ m

4.5.3 Discussion

According to Figs. 2, 3, 4, 5, 6, and 7, we can reach some conclusions about the locations
and stability of the off-axis equilibrium points:

1. In these figures, the loci of equilibrium points and their stability have several symmetries.
They are symmetrical with respect to the equatorial principal axes $\boldsymbol{u}$- and $\boldsymbol{v}$-axes. This is due
to the symmetries of mass distributions of the asteroid and spacecraft. Besides, for a given
value of ψ, the equilibrium points and their stability are symmetrical with respect to the
center of the asteroid, and the two symmetrical equilibrium points have the same parameters
with each other. This symmetry has also been shown by Eqs. (47) and (48). Although in the
figures the stability is indicated by using texts only for some equilibrium points, the stability
of other equilibrium points is easy to know by these symmetries.

2. As ρ increases, the significance of GOACP $\boldsymbol{\alpha}_{OAC}$ also increases. Meanwhile, the shift
of equilibrium point from the equatorial principal axes becomes larger, and the effect of
GOACP on the stability of equilibrium points becomes more significant.

When $\rho = 2$ m, GOACP $\boldsymbol{\alpha}_{OAC}$ is weak. The system is close to the previous orbital dynamics without $\boldsymbol{\alpha}_{OAC}$, and the equilibrium points are near to those in the previous model given by Eqs. (24) and (25), as shown by Fig. 2. The stability is also close to that in previous orbital dynamics determined by the asteroid parameters μ, ω_T, τ_0 and τ_2 as in Eq. (26): By using Eq. (26) we know that the classical equilibrium points on the $\boldsymbol{v}$-axis are stable, and those on the $\boldsymbol{u}$-axis are unstable; We also know that in Fig. 2 all the off-axis equilibrium points near the $\boldsymbol{v}$-axis are stable, whereas all those near the $\boldsymbol{u}$-axis are unstable.

In Figs. 3, 4, and 5, as ρ increases to 120 m, the significance of GOACP $\boldsymbol{\alpha}_{OAC}$ increases. Consequently, the loci of equilibrium points expand from the vicinity of the classical equilibrium points without $\boldsymbol{\alpha}_{OAC}$, and the maximum shift of equilibrium points from the equatorial principal axes increases. Besides the locations, the stability property of equilibrium points also diverges from that in the previous dynamics without $\boldsymbol{\alpha}_{OAC}$: We can see that in the case of $\rho = 50$ m all equilibrium points near the $\boldsymbol{v}$-axis are stable and all the equilibrium points near the $\boldsymbol{u}$-axis are unstable, whereas when ρ increases to 100–120 m some equilibrium points near the $\boldsymbol{v}$-axis have become unstable, as shown by Figs. 4 and 5.

In Figs. 6 and 7, when ρ increases to 140–160 m, the loci of equilibrium points expand to two closed curves around the asteroid. That is to say, the equilibrium point can exist at an arbitrary longitude in the equatorial plane with an appropriate attitude angle ψ. The equilibrium points on the outer closed curve are all unstable. On the inner closed curve, the equilibrium points near the $\boldsymbol{u}$-axis are stable and those near the $\boldsymbol{v}$-axis are unstable. Compared with Figs. 2, 3, 4, and 5, we can find that the locations of the stable equilibrium points have moved from near the v-axis to near the $\boldsymbol{u}$-axis.

Therefore, by using GOACP $\boldsymbol{\alpha}_{OAC}$, the spacecraft can stay at an arbitrary longitude around the asteroid without orbital control at the stable equilibrium points or with small orbital control at the unstable ones. This result is totally different from the previous orbital dynamics without $\boldsymbol{\alpha}_{OAC}$, and it provides many potential applications for the asteroid proximity-operations. For example, the asteroid body-fixed hovering at an arbitrary longitude can be achieved by using GOACP $\boldsymbol{\alpha}_{OAC}$.

Also notice that in Figs. 6 and 7 as ρ increases from 140 to 160 m, GOACP becomes more significant. Consequently, the separation between the two closed curves increases.

3. As shown by Figs. 2, 3, 4, and 5 when ρ is about and smaller than 120 m, the loci of equilibrium points with respect to ψ are four symmetrical closed curves around the classical equilibrium points without $\boldsymbol{\alpha}_{OAC}$. As ρ increases, the closed curves become larger. For a given value of ψ, there exist four equilibrium points that are located on the four closed curves, respectively, and are symmetrical with respect to the asteroid center.

With the attitude angle ψ changing from 0 to π, the equilibrium point will move along the closed curve for one cycle. When ψ changes from 0 to $\pi/2$, the equilibrium point will move off the asteroid principal axis, and after reaching the maximum shift it will move back towards and finally return to the asteroid principal axis when $\psi = \pi/2$. When ψ changes further from $\pi/2$ to π, the equilibrium point will move off the equatorial principal axis on the opposite direction.

The locus between $\psi = \pi/2$ and $\psi = \pi$ is symmetrical with that between $\psi = 0$ and $\psi = \pi/2$ with respect to the asteroid principal axis. The equilibrium point will return to the starting point $\psi = 0$ on the asteroid principal axis when $\psi = \pi$. The two equilibrium points on the asteroid principal axis when $\psi = 0(\pi)$ and $\psi = \pi/2$, which are actually on-axis equilibrium points, correspond to the cases that the $\boldsymbol{i}$- and $\boldsymbol{j}$-axes of the spacecraft are parallel to the asteroid principal axis, respectively.

In the cases of $\rho = 100$ m and $\rho = 120$ m, as the equilibrium point moves along the closed curve near the $\boldsymbol{v}$-axis, the stability property can be changed.

4. As shown by Figs. 5 and 6, when ρ increases from 120 to 140 m, the loci of equilibrium points have fundamental changes.

When ρ increases from 120 to 140 m, the starting point $\psi = 0$ and the ending point $\psi = \pi$ of the two closed curves crossing the $\boldsymbol{u}$-axis in Fig. 5 "jump" from the $\boldsymbol{u}$- to $+\boldsymbol{v}$-axis and $-\boldsymbol{v}$-axis in Fig. 6, and then these two closed curves in Fig. 5 become two open curves connecting the asteroid's $+\boldsymbol{v}$- and $-\boldsymbol{v}$-axes in Fig. 6. These two open curves form the outer closed curve around the asteroid, which means that the equilibrium point can exist at an arbitrary longitude with an appropriate attitude angle ψ.

At the same time, the starting point $\psi = 0$ and the ending point $\psi = \pi$ of the two closed curves crossing the $\boldsymbol{v}$-axis in Fig. 5 "jump" to $+\boldsymbol{u}$- and $-\boldsymbol{u}$-axis in Fig. 6, and then these two closed curves crossing the $\boldsymbol{v}$-axis in Fig. 5 become two open curves connecting the asteroid's $+\boldsymbol{u}$- and $-\boldsymbol{u}$-axes in Fig. 6. These two open curves also form a closed curve, the inner one, which also means that the equilibrium point can exist at an arbitrary longitude with an appropriate attitude angle ψ.

We can see that when the locations of equilibrium points have fundamental changes from Fig. 5 to Fig. 6, the stability property has followed the equilibrium points: the locations of the stable equilibrium points have moved from near the v-axis to near the $\boldsymbol{u}$-axis.

4.5.4 Attitude stabilization

As shown above, the asteroid body-fixed hovering at an arbitrary longitude can be achieved at the off-axis equilibrium points by using GOACP $\boldsymbol{\alpha}_{OAC}$.

However, in the attitude-restricted orbital dynamics, we have assumed that the spacecraft is controlled ideally to a given attitude with respect to the asteroid. At the off-axis equilibrium points, the spacecraft attitude is biased with respect to the nadir direction; therefore, the spacecraft will suffer from a constant gravity gradient torque caused by the asteroid gravity. The angular momentum caused by this constant gravity gradient torque needs to be absorbed consistently by the onboard attitude control system, i.e., the reaction wheels. When the angular momentum of the reaction wheels reaches saturation, fuel will be needed for the unloading. Therefore, it is necessary to assess the effect of the gravity gradient torque to see how much fuel will be needed to unload the angular momentum of the reaction wheels.

The second-order gravity gradient torque acting on the spacecraft expressed in its body-fixed frame S_B can be given by

$$T = \frac{3\mu}{R^5} R \times I R, \tag{53}$$

where $\boldsymbol{R} = \boldsymbol{A}^T \boldsymbol{r}$ is the position vector with respect to the asteroid expressed in the spacecraft body-fixed frame S_B. Since the relative attitude A with respect to the asteroid is a single axis rotation around the $\boldsymbol{w}$-axis, see Eq. (38), the position vector $\boldsymbol{R}$ is within the $\boldsymbol{i}$–$\boldsymbol{j}$ plane of the spacecraft, and then the gravity gradient torque $\boldsymbol{T}$ has non-zero component only on the $\boldsymbol{k}$-axis of the spacecraft with its components on the $\boldsymbol{i}$- and $\boldsymbol{j}$-axes both equal to zero.

We have calculated the magnitude of gravity gradient torque per unit mass (kg) of the spacecraft for the off-axis equilibrium points in Figs. 2, 3, 4, 5, 6, and 7. Curves of magnitude of the gravity gradient torque per unit mass (kg) with respect to the attitude angle $0 \leq \psi \leq \pi$ in the cases of six different values of ρ are given in Fig. 8. For each value of ρ, there are two curves corresponding to the two groups of off-axis equilibrium points that are not symmetrical with respect to the asteroid center.

Fig. 8 Magnitude of gravity gradient torque per unit mass (kg) of spacecraft at off-axis equilibrium points
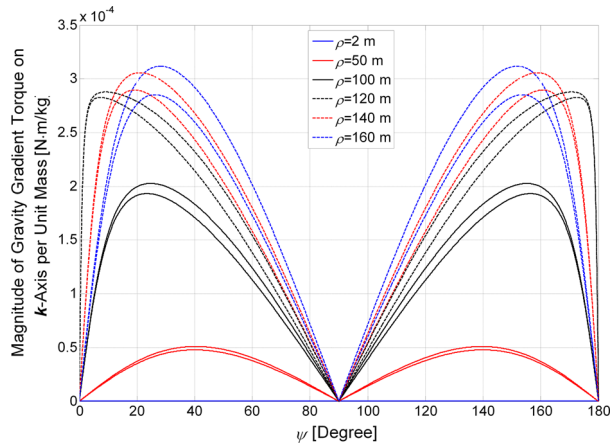
We can find that as ρ increases, the magnitude of gravity gradient torque also increases. In the case of $\rho = 2$ m the magnitude of gravity gradient torque is too small to be seen in Fig. 8. In the case of $\rho = 160$ m the maximum magnitude of gravity gradient torque per unit mass (kg) of the spacecraft is about 3×10^{-4} N m/kg. In worst case, all the absorbed angular momentum by the reaction wheels needs to be unloaded by the thrusters. The average control acceleration by the thrusters to unload the angular momentum can be estimated as about $3 \times 10^{-4}/\rho = 1.8750 \times 10^{-6}$ m/s^2, which is practical. In a better case, before the wheels reach saturation, the angular momentum can be stored temporarily by the wheels and can be unloaded by the gravity gradient torque with the opposite direction in later mission operations. Therefore, the asteroid body-fixed hovering at the off-axis equilibrium points by using GOACP α_{OAC} is practical in space engineering.

5 Conclusions

We have added GOACP into the close-proximity orbital dynamics about asteroids for a large spacecraft to improve the previous orbital models. By assuming that the spacecraft attitude is controlled ideally with respect to the asteroid, we have proposed a new orbital dynamics model called the attitude-restricted orbital dynamics.

Two kinds of equilibrium points within the asteroid equatorial plane are discovered: on- and off-axis. On-axis equilibrium points are located on the asteroid equatorial principal axes, and require one of the principal axes of the spacecraft to be parallel to the equatorial principal axis. The existence of off-axis equilibrium points, which cannot exist in previous orbital models, is attributed to GOACP. Off-axis equilibrium points within the equatorial plane require that one of the spacecraft principal planes is parallel to the equatorial plane. Locations of the off-axis equilibrium points depends on the relative attitude of spacecraft, and the loci of equilibrium points with respect to the attitude vary with the spacecraft characteristic dimension. In the case of an enough large characteristic dimension, the off-axis equilibrium points can exist at an arbitrary longitude in the equatorial plane with an appropriate attitude.

Our results have shown that, because of GOACP, the phase space of attitude-restricted orbital dynamics is much more complicated than that of the previous close-proximity orbital dynamics. The equilibrium points can give a basic picture of the phase space. More importantly, the spacecraft can stay at stable equilibrium points without orbital control and stay at

unstable equilibrium points with small control without needing to null out the unbalanced gravity. Therefore, the equilibrium points are useful for the asteroid close-proximity operations. The asteroid body-fixed hovering at an arbitrary longitude can be achieved at the off-axis equilibrium points by using GOACP without or with small orbital control.

The location and attitude of the spacecraft at equilibrium points depends on its mass distribution. In the future, it is of great interest to study how to modify the mass distribution (shape) of the spacecraft, such as by using deployable appendices, to affect its position and attitude at the equilibrium points.

References

Fahnestock, E.G., Scheeres, D.J.: Dynamical characterization and stabilization of large gravity tractor designs. J. Guid. Control Dyn. **31**(3), 501–521 (2008)

Früh, C., Kelecy, T.M., Jah, M.K.: Coupled orbit–attitude dynamics of high area-to-mass ratio (HAMR) objects: influence of solar radiation pressure, Earth's shadow and the visibility in light curves. Celest. Mech. Dyn. Astron. **117**(4), 385–404 (2013)

Hu, W.: Orbital Motion in Uniformly Rotating Second Degree and Order Gravity Fields. Ph.D. dissertation, Department of Aerospace Engineering, The University of Michigan, Michigan (2002)

Hu, W., Scheeres, D.J.: Numerical determination of stability regions for orbital motion in uniformly rotating second degree and order gravity fields. Planet. Space Sci. **52**, 685–692 (2004)

Jiang, Y., Baoyin, H., Li, J., et al.: Orbits and manifolds near the equilibrium points around a rotating asteroid. Astrophys. Space Sci. **349**(1), 83–106 (2014)

Kumar, K.D.: Attitude dynamics and control of satellites orbiting rotating asteroids. Acta Mech. **198**, 99–118 (2008)

Lee, D., Sanyal, A.K., Butcher, E.A., Scheeres, D.J.: Almost global asymptotic tracking control for spacecraft body-fixed hovering over an asteroid. Aerosp. Sci. Technol. **38**, 105–115 (2014)

Li, X., Qiao, D., Cui, P.: The equilibria and periodic orbits around a dumbbell-shaped body. Astrophys. Space Sci. **348**(2), 417–426 (2013)

Liu, X., Baoyin, H., Ma, X.: Equilibria, periodic orbits around equilibria, and heteroclinic connections in the gravity field of a rotating homogeneous cube. Astrophys. Space Sci. **333**, 409–418 (2011a)

Liu, X., Baoyin, H., Ma, X.: Periodic orbits in the gravity field of a fixed homogeneous cube. Astrophys. Space Sci. **334**, 357–364 (2011b)

Llanos, P.J., Miller, J.K., Hintz, G.R.: Orbital evolution and environmental analysis around asteroid 2008 EV5. In: The 24th AAS/AIAA Space Flight Mechanics Meeting, AAS 14-360, Santa Fe, NM, USA, January 26–30 (2014)

McMahon, J.W., Scheeres, D.J.: Dynamic limits on planar libration–orbit coupling around an oblate primary. Celest. Mech. Dyn. Astron. **115**, 365–396 (2013)

Misra, A.K., Panchenko, Y.: Attitude dynamics of satellites orbiting an asteroid. J. Astronaut. Sci. **54**(3&4), 369–381 (2006)

Misra, G., Izadi, M., Sanyal, A., Scheeres, D.J.: Coupled orbit–attitude dynamics and pose estimation of spacecraft near small solar system bodies. Adv. Space Res. (2015) **(accepted)**

Riverin, J.L., Misra, A.K.: Attitude dynamics of satellites orbiting small bodies. In: AIAA/AAS Astrodynamics Specialist Conference and Exhibit, AIAA 2002-4520, Monterey, CA, USA, 5–8 August (2002)

Russell, R.P.: Survey of spacecraft trajectory design in strongly perturbed environments. J. Guid. Control Dyn. **35**(3), 705–720 (2012)

Sanyal, A.K.: Dynamics and Control of Multibody Systems in Central Gravity. Ph.D. dissertation, Department of Aerospace Engineering, The University of Michigan, Ann Arbor, MI, USA (2004)

Sanyal, A., Izadi, M., Misra, G., Samiei, E., Scheeres, D.J.: Estimation of dynamics of space objects from visual feedback during proximity operations. In: AIAA/AAS Astrodynamics Specialist Conference, AIAA 2014-4419, San Diego, CA, USA, August 4–7 (2014)

Segal, S., Gurfil, P.: Effect of kinematic rotation–translation coupling on relative spacecraft translational dynamics. J. Guid. Control Dyn. **32**(3), 1045–1050 (2009)

Scheeres, D.J.: Dynamics about uniformly rotating triaxial ellipsoids: applications to asteroids. Icarus **110**, 225–238 (1994)

Scheeres, D.J.: Stability of relative equilibria in the full two-body problem. Ann. N.Y. Acad. Sci. **1017**, 81–94 (2004)

Scheeres, D.J.: Relative equilibria for general gravity fields in the sphere-restricted full 2-body problem. Celest. Mech. Dyn. Astron. **94**(3), 317–349 (2006)

Scheeres, D.J.: Stability of the planar full 2-body problem. Celest. Mech. Dyn. Astron. **104**, 103–128 (2009)

Scheeres, D.J.: Orbit mechanics about asteroids and comets. J. Guid. Control Dyn. **35**(3), 987–997 (2012a)

Scheeres, D.J.: Orbit mechanics about small bodies. Acta Astronaut. **72**, 1–14 (2012b)

Scheeres, D.J.: Close proximity dynamics and control about asteroids. In: 2014 American Control Conference (ACC), Portland, OR, USA, June 4–6 (2014)

Sincarsin, G.B., Hughes, P.C.: Gravitational orbit–attitude coupling for very large spacecraft. Celest. Mech. **31**, 143–161 (1983)

Teixidó Román, M.: Hamiltonian Methods in Stability and Bifurcations Problems for Artificial Satellite Dynamics. Master thesis, Facultat de Matemàtiques i Estadística, Universitat Politècnica de Catalunya, pp. 51–72 (2010)

Wang, Y., Xu, S.: Attitude stability of a spacecraft on a stationary orbit around an asteroid subjected to gravity gradient torque. Celest. Mech. Dyn. Astron. **115**(4), 333–352 (2013a)

Wang, Y., Xu, S.: Equilibrium attitude and nonlinear stability of a spacecraft on a stationary orbit around an asteroid. Adv. Space Res. **52**(8), 1497–1510 (2013b)

Wang, Y., Xu, S.: Symmetry, reduction and relative equilibria of a rigid body in the J2 problem. Adv. Space Res. **51**(7), 1096–1109 (2013c)

Wang, Y., Xu, S.: Stability of the classical type of relative equilibria of a rigid body in the J2 problem. Astrophys. Space Sci. **346**(2), 443–461 (2013d)

Wang, Y., Xu, S.: Gravitational orbit–rotation coupling of a rigid satellite around a spheroid planet. J. Aerosp. Eng. **27**(1), 140–150 (2014a)

Wang, Y., Xu, S.: Relative equilibria of full dynamics of a rigid body with gravitational orbit–attitude coupling in a uniformly rotating second degree and order gravity field. Astrophys. Space Sci. **354**(2), 339–353 (2014b)

Wang, L.-S., Krishnaprasad, P.S., Maddocks, J.H.: Hamiltonian dynamics of a rigid body in a central gravitational field. Celest. Mech. Dyn. Astron. **50**, 349–386 (1991)

Wang, L.-S., Maddocks, J.H., Krishnaprasad, P.S.: Steady rigid-body motions in a central gravitational field. J. Astronaut. Sci. **40**, 449–478 (1992)

Wang, Y., Xu, S., Tang, L.: On the existence of the relative equilibria of a rigid body in the J2 problem. Astrophys. Space Sci. **353**(2), 425–440 (2014a)

Wang, Y., Xu, S., Zhu, M.: Stability of relative equilibria of the full spacecraft dynamics around an asteroid with orbit–attitude coupling. Adv. Space Res. **53**(7), 1092–1107 (2014b)

Woo, P., Misra, A.K., Keshmiri, M.: On the planar motion in the full two-body problem with inertial symmetry. Celest. Mech. Dyn. Astron. **117**(3), 263–277 (2013)

Yu, Y., Baoyin, H.: Generating families of 3D periodic orbits about asteroids. Mon. Not. R. Astron. Soc. **427**(1), 872–881 (2012a)

Yu, Y., Baoyin, H.: Orbital dynamics in the vicinity of asteroid 216 Kleopatra. Astron. J. **143**(3), 62 (2012b)

Yu, Y., Baoyin, H.: Resonant orbits in the vicinity of asteroid 216 Kleopatra. Astrophys. Space Sci. **343**(1), 75–82 (2013)

Zhang, M.J., Zhao, C.Y.: Attitude stability of a spacecraft with two flexible solar arrays on a stationary orbit around an asteroid subjected to gravity gradient torque. Astrophys. Space Sci. **351**(2), 507–524 (2014)

Zhang, M.J., Zhao, C.Y.: Attitude stability of a dual-spin spacecraft on a stationary orbit around an asteroid subjected to gravity gradient torque. Astrophys. Space Sci. **355**(2), 203–212 (2015)